Table of contents:

1 Response to Anonymous Referee #1 2

2 New datasets 11

3 Dark light sensitivity 12

4 Statistical variations in the high frequency measurements 14

S1 Monte Carlo radiative transfer model 15

S1.1.1 Optical path length 15

S1.1.2 Scattering phase function 16

S1.1.3 Photon termination 16

S1.2 Monte Carlo experiment 17

S1.2.1 Source function for cosine detector 18

S1.2.2 Scattering and absorption by detector rod 19

S2 Model validation 20

S3 Monte Carlo uncertainty estimate 21

References 24

1 Response to Anonymous Referee #1

Received and published: 30 May 2020

General comments

Within the manuscript, spectral measurements of light attenuation in Greenland Ice Sheet bare ice are presented. For this purpose, the authors employed spectral irradiance measurements between 350-900 nm wavelength at the surface and at four different depths below the ice surface and calculated the spectral transmittance within the ice. From this, spectral flux attenuation and absorption coefficients are derived and compared to previous studies

The manuscript is clearly structured and the figures are of good quality, which helps to convey the arguments of the authors. The measurements of in-ice spectral transmittance are very valuable, and the author's efforts to put them into context and to identify possible future applications should be acknowledged. However, there are some aspects that need further focus in my opinion. After some general comments, the more specific comments and suggestions for technical corrections follow below.

Author reply: Thank you for your detailed comments on our manuscript. We believe we have addressed all of your concerns. In particular, we include a new detailed assessment of instrumental, measurement, and statistical uncertainty that we believe will substantially improve the usefulness of our findings.

Reviewer comment: In my point of view, the most pressing aspect is the lack of accounting for measurement uncertainties within the manuscript. So far, only statistical variations along the 30 measured irradiance spectra are considered, which need to be clearly separated from instrument uncertainties. However, the latter are not mentioned at all within the manuscript.

I suggest to include a new subsection within the 'Methods'-section that is devoted to instrument and measurement uncertainties. I understand the instrument is calibrated for irradiance measurements, but instrument errors such as the influence of dark and stray light, the wavelength calibration of the spectrometer, the non-ideal cosine response of the RCR diffuser, and the uncertainty of the absolute calibration (to get calibrated irradiance measurements) need to be quantified. Furthermore, as the transmittance is measured calculating the ratio of measured irradiance from two different instruments (the one in the ice, and the permanent one at the surface), differences between the two instruments need to be quantified (e.g., by means of a cross-calibration with the same light source). These instrumental errors need to be put in relation to uncertainties regarding the measurement setup (e.g., is the cosine receptor really in close contact with the ice during the in-ice irradiance measurements?) and the statistical variations as deduced from the 30 subsequently measured spectra.

Author reply: We appreciate this request for an uncertainty analysis. We addressed this by comparison with additional field datasets (Fig. 1) and with simulations from a 3-dimensional Monte Carlo radiative transfer model (Sect. S1 of this document).

Based on our Monte Carlo, we estimate an uncertainty on k_{att} due to the combined effects of detector rod interference and the non-ideal cosine response of the irradiance sensor diffusing element on the order 0.09–0.31 m^{-1} for the wavelength range 400–700 nm. Stated in terms of e-folding length scale, this uncertainty range is 9–90 mm.

Based on analysis of field datasets, we estimate an uncertainty on k_{att} due to dark-light sensitivity on the order 0.02–0.2 m^{-1} for the wavelength range 350–700 nm, or 5–20 mm in e-folding length scale (Fig. 2 and Fig. 3).

For comparison, the uncertainty deduced from statistical variations in the measured in-ice irradiance is of the order 0.007–0.23 m^{-1} at the two-sigma level, or 8–25 mm in e-folding length scale. The higher end of this uncertainty range applies to a small wavelength range near 700 nm. In the 400–600 nm range, the uncertainty is 0.005–0.007 m^{-1} (Fig. 4).

If the combined uncertainty addressed by Monte Carlo is taken as independent of the other estimates, an overall systematic uncertainty on k_{att} is 0.09–0.38 m^{-1} for the wavelength range 350–700 nm, estimated as:

$$\varepsilon = \sqrt{\varepsilon_{MC}^2 + \varepsilon_D^2 + \varepsilon_{2\sigma}^2}$$

where ε_{MC}, ε_D, and $\varepsilon_{2\sigma}$ are the uncertainty estimates for detector interference (estimated with Monte Carlo), dark-light sensitivity (estimated with field datasets), and statistical variations in the measured irradiances (estimated with field datasets), respectively. For comparison, the uncertainty in the linear regression, quantified as one standard error in the regression slope, is 0.05–0.22 m^{-1}. The specific methods used to estimate ε_{MC}, ε_D, and $\varepsilon_{2\sigma}$ are described in the new uncertainty analysis section in the Methods and Results, as requested.

For additional insight into experimental uncertainty, the revised manuscript includes a second attenuation coefficient (k_{att}) spectrum from measurements collected on 21 July, one day after the 20 July experiment described in the submitted manuscript. The 21 July in-ice irradiance data were collected at depths between 53–124 cm below the ice surface, whereas the 20 July data were collected at depths between 12–77 cm below the ice surface (Fig. 1).

The 21 July k_{att} values are nearly identical to the 20 July values at wavelengths between 600–650 nm but are lower by 0.06–0.13 m^{-1} in the 400–600 nm range. The lower k_{att} values at these visible wavelengths is consistent with the expectation that attenuation in deeper ice is less influenced by light absorbing material near the ice surface, whereas the nearly identical values at ~600 nm is consistent with the expectation that attenuation is dominated by ice absorption at near-infrared wavelengths. Differences between the 20 July and 21 July k_{att} spectra therefore likely reflect differences in the vertical variation of light absorbing material within the ice volume rather than instrumental and/or measurement uncertainty.

Overall, this comparison supports our experimental conclusions and gives additional insight into the relative influence of light absorbing material on variations in attenuation magnitude. More details are given in relevant sections below. The Monte Carlo model is described in the attached supplementary document.

Reviewer comment: This uncertainty analysis should eventually lead to vertical uncertainty bars in Figure 3, together with the horizontal uncertainty bars stemming from the depth measurements with the ruler (this second paragraph of Section 3.5 should also be moved to the new uncertainty subsection in Section 'Methods'). The errors in the linear regression to derive the flux attenuation coefficient should consider both depth and transmittance uncertainty estimates and, eventually, should lead to an uncertainty range attributed to each k_{att} value. A thorough treatment of the measurement uncertainties will definitely increase the value of the measurements for further applications.

Author reply: As requested, a new uncertainty subsection has been added to Methods that describes the new measurement uncertainty estimates given above. These new values have been added as vertical uncertainty on the reported k_{att} spectra (Fig 8). Please also see Section S1 of this document (where Fig. 8 is located) that summarizes the new uncertainty estimate, as requested.

Reviewer comment: Another remark is more structural and concerns the introduction of figures in the text: Some figures need to be described and explained in more detail within the text already. So far, some figures are mentioned for the first time in the text in brackets after an interpretation of the figure is done already. In contrast, the figure captions explain the figures in a lot of detail. I suggest providing the information of the figure captions already within the text of the manuscript.

Author reply: We moved the detailed descriptions from the figure captions to the main text, as requested.

Reviewer comment: It is definitely fair to point out that the presented measurements are a valuable contribution to the field as (to my knowledge) such experimental values do not exist for glacier ice. However, the authors should consider to not oversell their work in mentioning it many times throughout the manuscript (e.g., the title, and on Page 2 Line 41, P3 L72, P3 L89, ...). In a somewhat related issue, the title reads a bit 'bulky' and would benefit from being shortened in my opinion. However, this is of course only something to consider for the authors. In addition,

some shortcomings in explaining the applied methodology should be fixed in order to increase reading comprehension and reproducibility of the measurements (see specific comments below).

Author reply: We removed the claim "First" from the title and throughout the text, to reduce perceptions of overselling the work. We also removed the reference to ICESat-2. The new title reads: "Spectral attenuation coefficients from measurements of light transmission in bare ice on the Greenland Ice Sheet".

Specific comments

Introduction

• Page 2 Line 46: at this point of the introduction, it is helpful to give some values for typical ranges of air bubble and ice grain sizes.

Author reply: We added values for near-surface glacier ice air bubble and grain-size radii, which are of the order 10^{-2}–10^{-3} m, or 10^{-1}–10^{-3} m in terms of optically-equivalent grain size (Dadic et al., 2013), as requested.

• P3 L66: While it is true that analytical models typically assume spherical scatterers to calculate the inherent optical properties, the introduction should also point at different approaches and mention efforts by Kokhanovsky and Zege (2004) as well as Malinka (2014) and Malinka et al. (2016) which provide analytical solutions for single-scattering properties but model snow and ice grains as nonspherical.

Author reply: Thank for these suggestions. We added a discussion of these important studies to the Introduction, as requested:

Kokhanovsky, A. A. and Zege, E. P.: Scattering optics of snow, Appl. Opt., 43, 1589–1602, https://doi.org/10.1364/AO.43.001589, 2004.

Malinka, A.: Light scattering in porous materials: Geometrical optics and stereological approach, J. Quant. Spectrosc. Radiat. Transf., 141,3514–23, https://doi.org/10.1016/j.jqsrt.2014.02.022,, 2014.

Malinka, A., Zege, E., Heygster, G., and Istomina, L.: Reflective properties of white sea ice and snow, Cryosphere, 10, 2541–2557,https://doi.org/10.5194/tc10-2541-2016, 2016.

Methods

• How did you make sure the cosine receptor is in direct contact with the ice to avoid another ice-air interface? Shimming the ruler underneath the PVC tube seems to help, but have you done any testing in that regard?

Author reply: We did not perform optical measurements to test this. Our Monte Carlo simulations quantify the impact of scattering and absorption by the rod, which include the RCR as a scattering surface with the same optical properties as the rod (Sect. S1).

• P4 L123: This sentence reads a bit confusing to me and needs to be reformulated. Also: I don't understand the integration time given in Hertz I think a conversion to an actual time period is useful here.

Author reply: The 44 Hz corresponds to 0.0228 s integration time per scan. We agree this is confusing and the units for integration time are now reported in seconds, as requested.

The revised sentence reads: "Spectral irradiance was recorded at 1 Hz frequency. Each recorded measurement is a 20-scan average with 0.0228 s integration time per scan, yielding 0.4 s total integration time per irradiance measurement."

• I have some suggestions for Figure 1 that would help the reader in my opinion:

- the photograph of the measurement setup within Figure 1 should be enlarged (and maybe put to the right of the schematic) as, right now, it is a bit small.
- a horizontal line should clearly mark the ice surface, as due to the color gradient it is hard to distinguish from the end of the schematic.
- Can you indicate the other vertical positions of the transmittance measurements maybe with some dashed horizontal lines and then also draw an arrow indicating that the measurements were conducted from the bottom to the top?

Author reply: Each of these changes will be made to the revised figure, as requested.

• P5 L134: The weather situation during the measurements needs to be specified with respect to clouds, temperature, etc.

Author reply: The weather situation is expanded upon in the revised manuscript. The conditions were overcast with light rain on 20 July and overcast with partial cloud cover during some periods of the experiment on 21 July.

Results

• Figure 2

- It would be interesting to include the surface downwelling irradiance at z_0 into Figure 2a for comparison.

  Author reply: We added the surface downwelling irradiance to Figure 2a, as requested.

- The unit for the standard deviation is missing in Figure 2b.

  Author reply: We added the units, as requested.

- Figure caption: instead of naming it relative irradiance for the first time, I would name it Transmittance like in the rest of the manuscript.

  Author reply: We changed relative irradiance to transmittance, as requested.

• Figure 2b is not discussed in Section 3.1. Instead of stating in the Figure caption of Fig. 2b that the standard deviation is below 1 W m-2 nm-1 at all wavelengths, I would move this statement to the main text.

Author reply: We moved this statement to the main text in Section 3.1, as requested.

• P8 L216: Albedo is mentioned for the first time. Please explain at this point how it was calculated from the surface measurements.

Author reply: We added the definition of albedo and how we calculated it to the Methods Sect. 2.2, as requested.

The sentence reads: "The ice surface albedo was estimated as the ratio of the 2 m background upwelling spectral irradiance to the downwelling spectral irradiance. These irradiance data were smoothed with the same 1 nm

interpolation filter described above [for the in-ice irradiance measurements]. The ice surface albedo is presented in Sect. 3 to qualitatively discuss the in-ice irradiance measurements and the $k_{\mathrm{att}}(\lambda)$ estimates."

• P8 L231-...: Warren et al. (2006) also show the snow transmission measurements before removing the absorption by impurities wouldn't using these measurements lead to a similar discrepancy between the theory and field estimate for clean snow than for the glacier ice at smaller wavelengths? I suggest to use the uncorrected measurements for snow as well within Figure 4a, so that it is consistent with the glacier ice measurements.

Author reply: We removed this figure because it is redundant with Fig. 8 (comparison of k_{att} spectra from sea ice and snowpack), as requested by reviewer 2.

• P9 L252: The derivation of as the root-mean-squared difference between measured and predicted transmitted irradiance should already be explained in the respective Section 2.5 in the Methods.

Author reply: We added the derivation to Sect. 2.5, as requested.

The sentence reads "We estimate $\chi(\lambda)$ as the value that minimizes the root-mean-squared-difference between measured and predicted transmitted irradiance, weighted equally at all depths. In addition, we estimate a single broadband value of χ that minimizes the root-mean-squared-difference between measured and predicted transmitted irradiance, weighted equally at all depths and all λ.".

• Again P9 L252: I have a general question to the -value you applied. As you state in the caption of Figure 5, 'the spectral dependence [of the relative error] suggests a contribution of absorption to near-surface attenuation enhancement'. This calls for a spectral value of , and indeed you mention at P9 L253, 'weighted equally at all depths and all ' indicating that you derived for each individual wavelength separately. Is this the case? If so, please state already in Equation (7) that is dependent on (which is the main difference to i_0 in my understanding). However, I get confused with the last sentence of the paragraph on P9 L253: it reads as if you apply only one value of = 15 % to all wavelengths. Please clarify this in the text. The same applies to P12 L354.

Author reply: We include the spectrally averaged value because large-scale models often need a single value for the visible and a single value for the infrared, or a single broadband value (Briegleb and Light, 2007; Liston and Winther, 2005). We now report spectral $\chi(\lambda)$ values in addition to the average value, as requested.

• Figure 5: The second empirical model you use, applying $I(z_0) = I(z_{12\mathrm{cm}})$, seems to perform best as it is only applied in the isotropic region of transmittance. Looking at the formulas in Figs. 5b and 5c for I_z, one could think the best possible solution for would be such that (1) = $I_{12\mathrm{cm}}$. Which is not possible in my understanding as the exponential part of the equation (namely the 'z') is different. To avoid this confusion, the equation in Fig. 5b needs to be adapted accordingly: $I_z = I_{12\mathrm{cm}}$ exp [k(z 12 cm)]

Author reply: It is correct that the formula in Fig. 5b needs to include the z-12cm offset. We corrected the equation, as requested.

• P9 L256: it is unclear to the reader how the effective k_{att}-values are derived using a finite-difference solution to Eq. (2) (also: contradictory, in the caption of Figure 6 it says Eq. 1)?

Author reply: We corrected the caption of Fig. 6 to point to Eq. 2, as requested.

The finite difference solution takes the form:

$$I_{\lambda,0-12\ \mathrm{cm}} = -\frac{1}{\Delta z}\log[I_{\lambda,z=12\ \mathrm{cm}} - I_{\lambda,z_0}]$$

where Δz = 12cm.

We use a centered finite difference (i.e. $1/\Delta z$) to estimate a bulk attenuation value for the 0–12 cm region. We specified this in the revised text.

• P9 L260: please state how exactly the effective k_{att}-values were combined for calculation of the effective penetration depth, e.g. give an equation for that.

Author reply: We added a new Eq. 8 that shows how these values are calculated, as requested.

Here is the equation:

From the definition of optical depth:

$$\tau_{\lambda,z} = \int_0^{z'} k_{\lambda,z} dz$$

we define a piecewise optical depth:

$$\tau_{\lambda,z} = \int_0^{12\ cm} k_{\lambda,0-12cm} dz + \int_{12\ cm}^{z'} k_\lambda dz$$

where $k_{\lambda,0-12\text{cm}}$ is the centered finite-difference estimate of k_{att} for $z_{0-12\text{cm}}$ and k_λ is the asymptotic k_{att} for $z_{12-77\text{cm}}$ estimated from the irradiance measurements.

The e-folding depth is the depth at which $\tau = 1$. Setting $\tau_\lambda = 1$ in Eq. X and solving for z' yields:

$$z' = \frac{1 - (k_{\lambda,0-12\ cm} \times 0.12) + (k_\lambda \times 0.12)}{k_\lambda} = 49 \text{ cm}$$

• P10 L280: Please clarify in more detail how the external diffuse specular reflectivity for a flat ice surface was calculated in this case.

Author reply: The formulas used to calculate the external diffuse specular reflectivity are described in Section S1.2.2 of the attached supplementary document: Monte Carlo uncertainty analysis, where we use the same formulas to calculate the specular reflection from the PVC detector rod. The formulas are repeated in brief here:

Let θ be the polar (zenith) angle between the flat ice surface and the unit normal and $\mu = \cos\theta$ be the cosine zenith angle. Following Modest (2013) Section 2.5 Eq. 2.89–2.98, the Fresnel reflectivity $R_F(\mu)$ and transmissivity $T_F(\mu)$ to incident (downward) radiation are:

$$R_F(\mu) = \frac{1}{2}\left[\left(\frac{\mu - n\mu_n}{\mu + n\mu_n}\right)^2 + \left(\frac{n\mu - \mu_n}{n\mu + \mu_n}\right)^2\right]$$

$$T_F(\mu) = 1 - R_F(\mu)$$

where $n + ik$ is the complex refractive index of ice and:

$$\mu_n = \sqrt{1 - (1 - \mu^2)/n^2}$$

is the refracted cosine zenith angle in the ice. The diffuse external reflectivity is obtained by integrating $R_F(\mu)$ across the incident hemisphere normalized by the incident flux:

$$R_F = \frac{1}{2}\int_0^1 \mu R_F(\mu) d\mu.$$

• Section 3.5: The title 'Uncertainty analysis' is misleading. It is true that the second paragraph of this section is a valuable uncertainty estimate, that should already be part of an 'Uncertainty analysis' subsection of the Section

'Methods' (compare general comment). The first paragraph of 3.5 is well-placed at this point of the manuscript, but I suggest to rename the subsection to e.g. 'Influence of ice density' after moving the second paragraph to the 'Methods'-section.

Author reply: As requested, we have renamed Section 3.5 and we have added an additional uncertainty analysis as a new Sect. 3.6: Monte Carlo uncertainty analysis, which is included as a supplement to this document.

• Figure 9: I suggest including an additional subsection that compares the k_{abs}values of this study with previous estimates. The first time the authors mention Figure 9 is in the 'Suggestions for further work' part, which definitely undersells this comparison. This is also a very specific case for what I was mentioning in the 'General comments' section: the Figure is mostly described and discussed in the Figure caption and not in the text at all. This should be changed.

Author reply: We added the additional subsection, as requested.

• P13 L394: The 'Further work ...'-part of the last sentence is not useful in my opinion, as Section 4.4 already gives suggestions for future studies. I would end the 'Conclusions' section with the new values of attenuation and absorption coefficients that are provided in this study.

Author reply: We replaced the last sentence with the new values of attenuation and absorption coefficients, as requested. The scattering coefficient is ~1.0 m^{-1} in the 350–500 nm range and increases to ~5.0 m^{-1} from 500–700 nm.

• Data availability: please provide the doi of the published dataset in Pangaea.

Author reply: The URL to the dataset is printed below. Please note that the dataset is considered "in review" as the parent work (this manuscript) remains in review. As per the policies of the data repository the DOI will remain unregistered until the work is published.

https://doi.pangaea.de/10.1594/PANGAEA.913508

Technical corrections

• P2 Eq. (1): please indicate the spectral dependence already within the equation.

Author reply: We added the spectral dependence to the equation.

• P2 L47: please make sure the exponents are not split up at a line break.

Author reply: Thank you for noting this. We replaced all units with non-breaking hyphens.

• P2 L61: as you specify the spectral dependence of m, you should include it also for m_{re} and m_{im}. In addition, naming them the real part and imaginary part of the complex index of refraction seems more appropriate than denoting them 'real and imaginary index'.

Author reply: We made the requested corrections.

• P2 L62: The authors should consider to give $k_{abs,ice}$ a separate, numbered equation.

Author reply: As requested, we added a separate numbered equation.

• P5 L139: The equation for the spectral transmittance should become a separate equation instead of an in-text equation.

Author reply: As requested, we made this a separate numbered equation.

• P6 L179: do you mean Warren and Brandt (2008)?

Author reply: Yes, thank you.

• P7 L183: Equation (2) does not give a direct relation to calculate $k_{att}()$. The authors should consider providing a separate equation for this purpose.

Author reply: We added the following relation as a separate equation, as requested:

"Estimates of $k_{\mathrm{att}}(\lambda)$ for each 1 nm band are estimated by solving a linear equation of the form:

$$-\log T(z,\lambda) = T_0 + k_{att}(\lambda)\cdot z + \varepsilon$$

where T_0 is a parameter (y-intercept) that represents $T(\mathrm{z}=0)$ and ε is an error term."

• Figure 3:

- The y-axes of Figs. 3a and 3b don't show the Transmittance T but its logarithm ln T please adjust the axes titles accordingly.

  Author reply: The data shown in Fig. 3a and 3b are transmittance plotted on log-scale axes. The axes are labeled correctly (consider that from any point on the line, trace horizontally to the y-axis, and the value obtained in this way is transmittance, not log transmittance).

- Legend for black line: 350 nm are stated in the text is '351 nm' a typing error?

  Author reply: Yes, this typing error has been corrected.

• P8 L220: the superscript 1 belongs to the unit of k_{att}, please keep it in one line.

Author reply: We replaced all units with non-breaking hyphens.

• P8 L234: reference should be to Figure 4a not Figure 5.

Author reply: We corrected the reference.

• P8 L236: 4 μm instead of 4 um.

Author reply: We corrected the symbol as requested.

• P9 L252: missing closing bracket after Eq. (7)

Author reply: We corrected this as requested.

• Figure 6: add y-axis title to Fig. 6b.

Author reply:

• P9 L273-274: don’t split the unit on different lines.

Author reply: We have replaced all units with non-breaking hyphens.

• P10 L281: I think this should be a reference to Fig. 3b.

Author reply: We corrected this reference to Fig. 3b.

• P10 L287: I guess you don’t mean ω?

Author reply: Thank you, this typo has been corrected. We intended to say “values of ω at wavelengths >800 nm”.

• P11 L310: to six previously published [...], not seven

Author reply: Thank you, this has been corrected.

• Bibliography: please add how to access the Mätzler (2002) and Perovich (1996) references.

Author reply: These URLs have been added to the references. They are:
Mätzler: https://boris.unibe.ch/146550/
Perovich: https://apps.dtic.mil/dtic/tr/fulltext/u2/a310586.pdf

• Appendix 1, P29 L693: the minus ’-’ in the unit is missing

Author reply: Thank you, this has been corrected.

2 New datasets

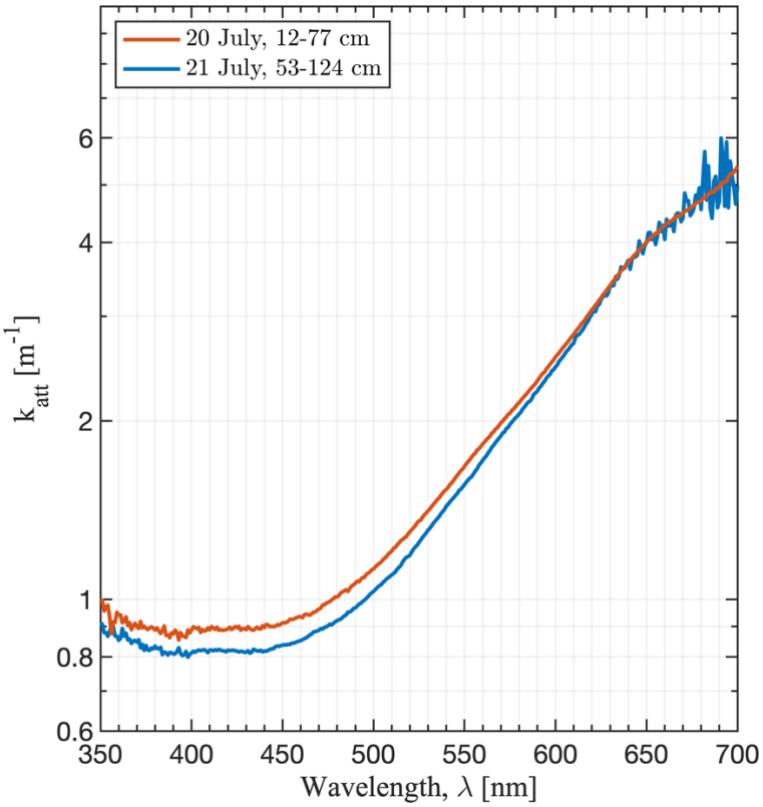

Fig. 1: k_{att} spectra calculated with in-ice irradiance collected on 20 July at depths between 12–77 cm below the ice surface and on 21 July at depths between 53–124 cm below the ice surface. The higher attenuation in the 12–77 cm depth region is consistent with the expectation that impurities have a larger impact on visible light attenuation nearer the ice surface. The close agreement in the 600–700 nm region is consistent with the expectation that ice absorption dominates attenuation in the near infrared. The noise in the 21 July spectrum at longer wavelengths is due to the lower light levels at those depths.

3 Dark light sensitivity

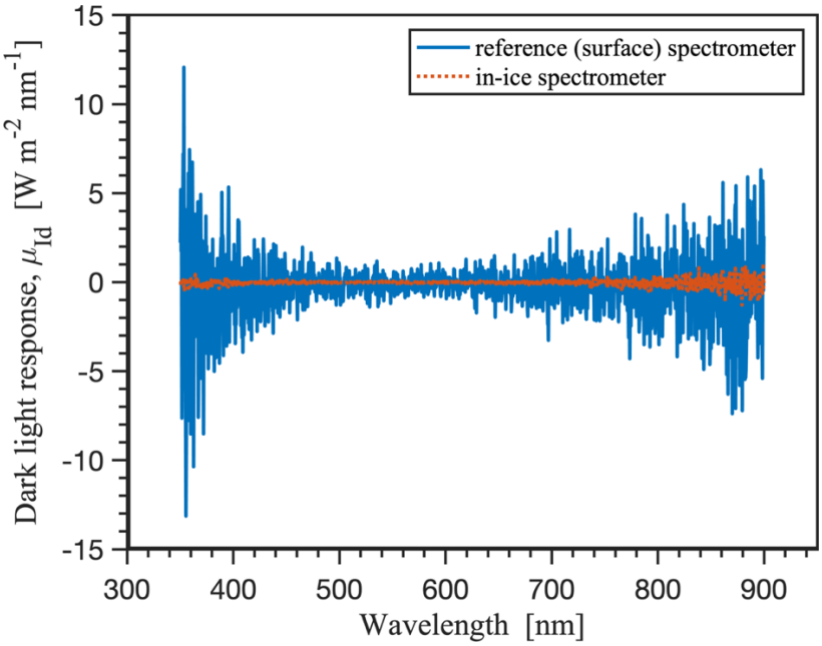

Fig. 2: Measured values of dark-light sensitivity collected with the reference spectrometer that was used to measure downwelling irradiance at 2 m height above the ice surface and with the spectrometer that was used to measure in-ice irradiance. The Ocean View software requires that a measurement of dark light is made prior to each absolute irradiance measurement, and automatically removes the dark light from the measured irradiance. The values shown in this figure represent the residual dark-light sensitivity that remained after the automated software correction. The dark light spectra shown here is subtracted from the irradiance measurements prior to fitting our experimental k_{att} values. Comparison of k_{att} computed with and without this dark-light correction is shown in Fig. 3.

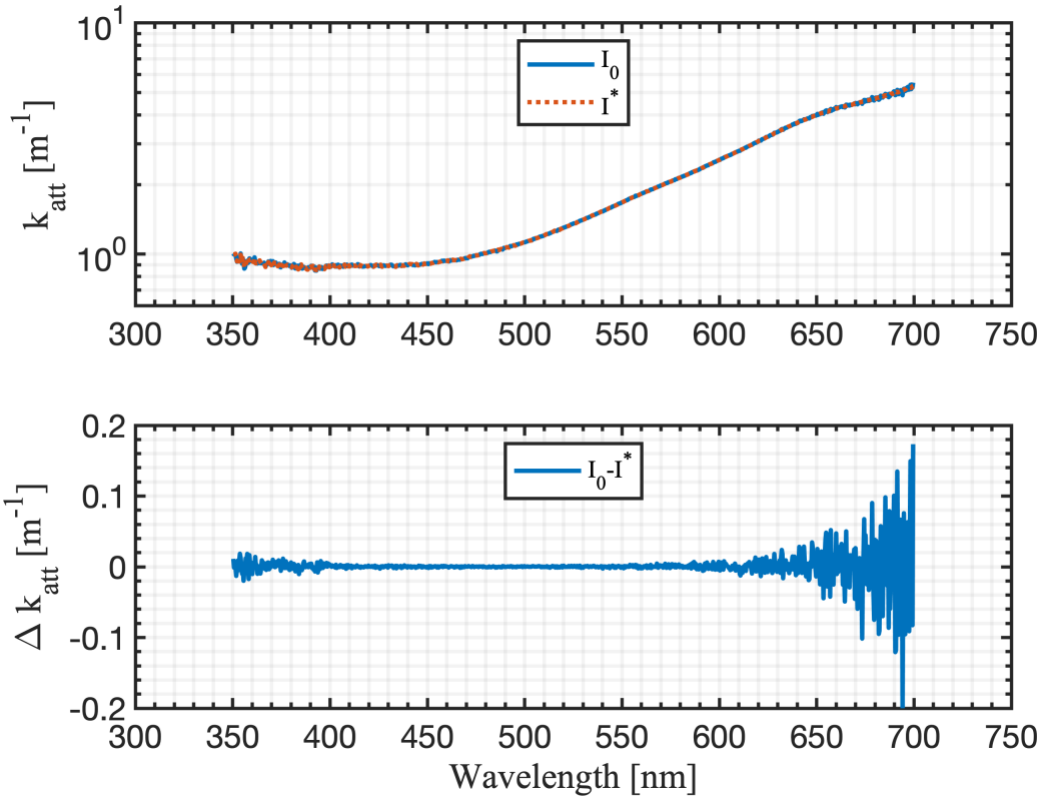

Fig. 3: (a) k_{att} spectra with (I*) and without (I_0) subtracting the dark-light response spectra shown in Fig. 2. (b) the difference between the two spectra in (a), which is used as an estimate of uncertainty due to dark light response ε_D.

4 Statistical variations in the high frequency measurements

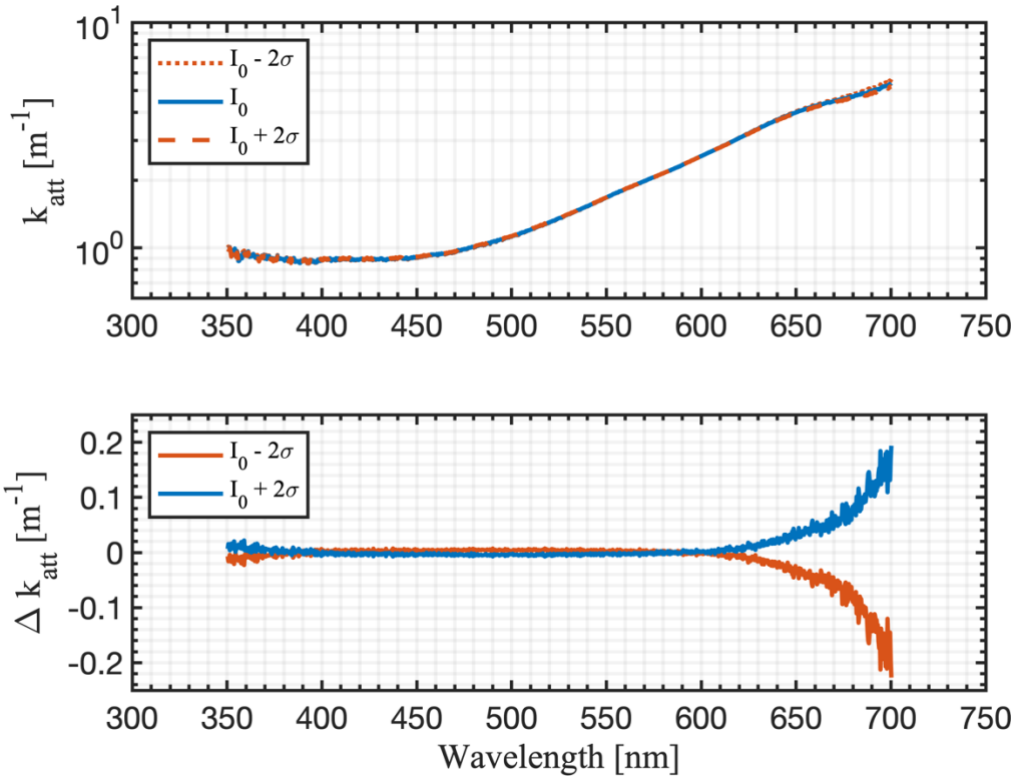

Fig. 4: (a) k_{att} spectra calculated by adding and subtracting two standard deviations in the high-frequency in-ice irradiance data at each depth from the mean value at each depth and re-calculating k_{att} with these modified irradiance values. (b) The difference between the two spectra in (a), which is used as an estimate of uncertainty due to high frequency variability in the irradiance measurements, $\varepsilon_{2\sigma}$.

S1 Monte Carlo radiative transfer model

The Monte Carlo method solves the radiative transfer equation (RTE) by simulating large ensembles of photon events represented by random samples from probability density functions (Ertürk and Howell, 2017). In this study and others, the Monte Carlo method is used to quantify relative uncertainties in imperfect optical measurements that are intractable with analytical or numerical solutions to the RTE (Gordon, 1985). We developed a Monte Carlo radiative transfer model to estimate the effect of detector interference on our irradiance measurements. The model closely follows methods developed to simulate light propagation in biological tissue, ocean waters, and sea ice (Leathers et al., 2004; Light et al., 2003; Wang et al., 1995). A general description of the model and particular modifications for this investigation are described below.

S1.1 Probability functions for optical properties

The fundamental ingredients of this and other Monte Carlo radiative transfer models are the inherent optical properties k, ω, and g (see Sect. 2.3 of the main), the geometric boundary conditions, and the probabilistic rules that govern the system. The cumulative probability of occurrence for an event x, with probability density function $\mathrm{p(x)}$, is:

$$\mathrm{P(x)} = \int_{-\infty}^{\mathrm{x}} \mathrm{p(x)dx}, \quad 0 \leq \mathrm{P(x)} \leq 1. \tag{1}$$

To solve for x, the left-hand-side (LHS) of (1) is replaced with a random number:

$$\mathrm{P(x)} = q \tag{2}$$

where q is from the uniform distribution over [0,1]. The right-hand-side (RHS) lower limit of integration $-\infty$ is replaced with an appropriate limit (e.g., 0) and analytic or empirical expressions for $\mathrm{p(x)}$ are specified.

In this study, x represents optical path length, scattering direction, and photon survival probability. Closed-form expressions for each of these terms are given in the following sections.

S1.1.1 Optical path length

The probability density function for the optical path length l [$\mathrm{m^{-1}}$] is given by the e-folding length:

$$\mathrm{p}(l) = \mathrm{e}^{-l}, \qquad l \geq 0 \tag{3}$$

with the cumulative distribution function:

$$\mathrm{P}(l) = \int_0^l \mathrm{e}^{-l'}\mathrm{d}l' = 1 - \mathrm{e}^{-l}. \tag{4}$$

From Eq. (2), $q = 1 - \mathrm{e}^{-l}$ and therefore:

$$l = -\ln q\,, \qquad 0 \leq 1. \tag{5}$$

In this study, q is generated with the MATLAB function rand.

The photon transport length [m] is the optical path length scaled by the extinction coefficient:

$$s = l/\sigma_e \tag{6}$$

where:

$$\sigma_e = \sigma_s + \sigma_a \tag{7}$$

is the single-scattering extinction coefficient, σ_s [m^{-1}] is the scattering coefficient, and σ_a [m^{-1}] is the absorption coefficient.

S1.1.2 Scattering phase function

The probability density function for a scattering phase function with azimuthal symmetry is:

$$p(\theta_s) = 2\pi\tilde{\beta}(\theta_s)\sin\theta \tag{8}$$

where $\tilde{\beta}(\theta_s)$ is the probability that a photon will scatter at polar angle θ_s. We specify $\tilde{\beta}(\theta_s)$ with the Henyey-Greenstein scattering phase function, which is appropriate for strongly forward scattering by ice grains and air bubbles (Light et al., 2003):

$$\tilde{\beta}(g, \theta_s) = \frac{1}{4\pi}\frac{1-g^2}{(1+g^2-2g\cos\theta_s)^{\frac{3}{2}}}, \qquad -1 < g < 1. \tag{9}$$

where $g = 0$ reduces Eq. 9 to isotropic scattering and $g \to 1$ is strongly forward scattering. In this study, $g = 0.86$, as given by Mullen & Warren (1988) from Mie theory calculations for scattering by air bubbles in ice.

From Eq. (1):

$$P(\theta_s) = -\frac{1-g^2}{2}\int_0^{\theta_s}\frac{\sin\theta_s'}{(1+g^2-2g\cos\theta_s')^{\frac{3}{2}}}d\theta_s' = q \tag{10}$$

which evaluates to:

$$q = \frac{1-g^2}{2g}\left[\frac{1}{1-g} - \frac{1}{\sqrt{1+g^2-2g\cos\theta_s}}\right] \tag{11}$$

yielding the scattering angle:

$$\cos\theta_s = \frac{1}{2g}\left[1+g^2-\left(\frac{1-g^2}{1-g+2gq}\right)^2\right], \qquad g \neq 0;\ 0 \le \theta_s \le \pi/2. \tag{12}$$

The probability density function for scattering azimuth angle ϕ_s in a spherical coordinate system with azimuthal symmetry is $1/2\pi$. From Eq. (1):

$$P(\phi_s) = \frac{\phi_s}{2\pi}, \qquad 0 \le \phi_s \le 2\pi \tag{13}$$

and from Eq. (2):

$$\phi_s = 2\pi q. \tag{14}$$

S1.1.3 Photon termination

Monte Carlo simulations are computationally expensive. To improve computational performance, photons are treated as packets of photons with initial weight $w = 1$. At each interaction, photons are scattered and absorbed according to their respective statistical probabilities, parameterized by σ_s and σ_a. Accordingly, at each interaction the weight is updated as:

$$w = (1 - \overline{\omega}) \cdot w \tag{15}$$

where:

$$\overline{\omega} = \sigma_\mathrm{s}/\sigma_e \tag{16}$$

is the single-scattering albedo [-]. Each $1 - \overline{\omega}$ reduction in photon packet weight is proportional to the probability of an individual photon absorption event. After many interactions, if w drops below a very small value it contributes very little to the solution. The so-called "Russian roulette" technique is used to improve computational performance, where photon packet weights below a specified threshold $w < w_\mathrm{min}$ are increased in proportion to a survival probability function and are re-released into the medium, or otherwise terminated:

$$w = \begin{cases} \mathrm{m} \cdot w, & q \leq 1/\mathrm{m} \\ 0, & q > 1/\mathrm{m} \end{cases} \tag{17}$$

where $1/\mathrm{m}$ is the probability of photon survival and q is a random number as previously defined. This technique conserves energy and is unbiased (Wang et al., 1995). In this study, $w_\mathrm{min} = 10^{-5}$ and $\mathrm{m} = 10$.

At each interaction, the absorbed fraction $\overline{\omega} \cdot w$ is scored into an absorption array in a cylindrical coordinate system that is used to compute observable quantities of absorption and photon fluence. If a photon packet exits the medium, it is scored into a transmittance or reflectance array in an azimuthally independent spherical coordinate system that is used to compute observable quantities of irradiance, radiant intensity, and power. These scoring systems follow the definitions in Wang et al. (1995) Eq. 4.1–4.32.

The preceding sections describe the fundamental processes of photon transport, scattering direction, and survival probability. Similar probability density functions that describe the detector rod interference are described next.

S1.2 Monte Carlo experiment

The detector rod interference is estimated with a "backward" Monte Carlo (BMC) simulation, which simulates photon trajectories starting from the detector backward to the target (Leathers et al., 2004; Light et al., 2003). Here, the target is the ice surface. The simulation domain is a 3-dimensional ice slab with one boundary, the ice surface, and otherwise infinite horizontal and vertical extent. A cylinder with dimensions identical to the detector rod is placed at positions identical to the measurement depths reported in this paper, and photon packets are released from the irradiance sensor ("remote cosine receptor") located on the detector rod (Fig. 5).

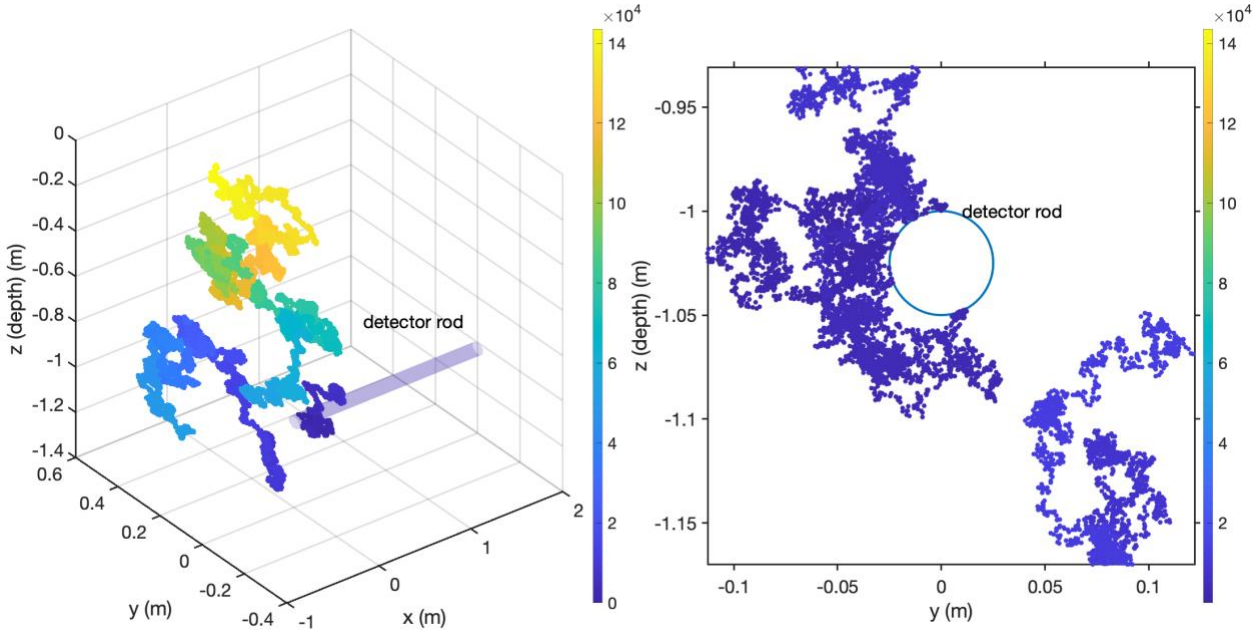

Fig. 5: Example Monte Carlo photon tracking simulation from model output used in this study, with interference by cylindrical detector rod. (a) ~14,000 random photon interactions are traced within a 3-dimensional ice volume. The cylindrical object represents the detector rod, here inserted at 1 m below the ice surface. The photon packet is released from the position of the irradiance sensor ("remote cosine receptor") located on the rod and traced backward to the ice surface ("backward Monte Carlo"). (b) Magnified view of the detector rod in the y-z plane shows photon packets scattering off of the rod. The color-bar represents the number of cumulative interactions experienced by this photon packet.

As described above, each interaction within the ice volume is defined by absorption and scattering of the photon by ice. Absorption reduces the photon energy density by an amount $1 - \overline{\omega}_{\mathrm{ice}}$. Scattering redirects the photon trajectory according to the Henyey-Greenstein scattering phase function with asymmetry parameter g and transport distance l. Photon interactions with the detector rod require additional specifications that are described next.

S1.2.1 Source function for cosine detector

The scattering phase function for an irradiance sensor with a cosine response is:

$$\tilde{\beta}(\theta) = \frac{\cos\theta}{\pi}, \qquad 0 \le \theta \le \frac{\pi}{2} \tag{18}$$

with probability density function:

$$p(\theta) = 2\pi\tilde{\beta}(\theta)\sin\theta \tag{19}$$

and cumulative distribution function:

$$P(\theta) = 2\int_0^{\theta} \cos\theta' \sin\theta' \, d\theta' = q\,. \tag{20}$$

Substituting $\mu = \cos(\theta)$ the scattering angle is:

$$\cos\theta = \sqrt{1-q}. \tag{21}$$

For a forward Monte Carlo simulation, Eq. 21 gives the probability of photon receipt by an irradiance sensor with an ideal cosine response. For a BMC simulation, the form of Equation 21 that gives the initial launch trajectory of photons from the irradiance sensor surface is:

$$\cos\theta = -\sqrt{q}. \tag{22}$$

In reality, irradiance sensors do not have an ideal cosine response to radiance. In this experiment, the non-ideal cosine response of the irradiance sensor is estimated by replacing Eq. 22 with uniform sampling from an empirical probability density function derived from laboratory measurements of the cosine receptor angular response function provided by Ocean Optics (Fig. 6). The source azimuth angle ϕ is determined with Eq. (14).

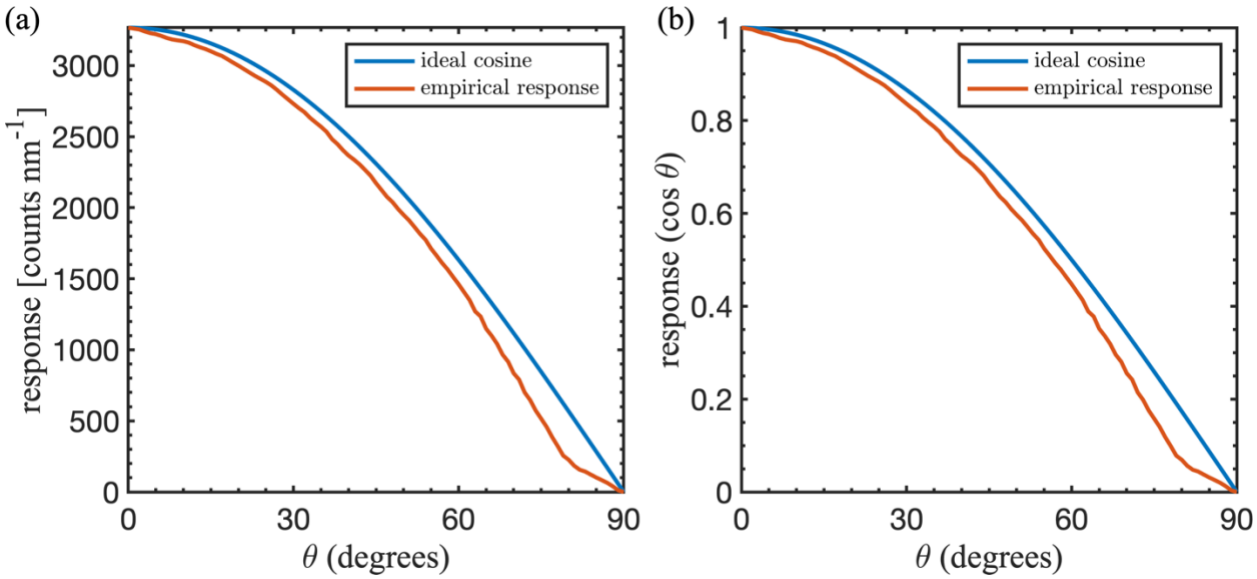

Fig. 6: (a) Comparison of ideal angular response function (ideal cosine) with the empirical angular response function used to estimate the non-ideal response of the irradiance sensor used in this study. The empirical angular response function was developed by Ocean Optics from laboratory measurements on the same irradiance sensor type used in this study. (b) Same as (a) but normalized. The red line in (b) is the empirical probability density function used as the irradiance source function for our backward-Monte Carlo simulations (see Eq. 21–22).

S1.2.2 Scattering and absorption by detector rod

If a photon trajectory crosses the 3-dimensional position of the detector rod, the photon energy density is reduced by an amount $1 - \omega_{\text{rod}}$ and the photon is scattered away from the rod (Fig. 5) with an isotropic scattering phase function:

$$\theta_s = 1 - 2q, \tag{23}$$

$$\phi_s = 2\pi q. \tag{24}$$

The collision point is determined with ray tracing formulas that equate the vector equation of the photon trajectory with the parametric equation for the cylindrical detector rod surface following Ertürk and Howell (2017) Sect. 7.1 Eq. 59–66.

The polyvinyl chloride (PVC) detector rod albedo ω_{rod} is estimated from values for the complex refractive index of PVC (Zhang et al., 2020). Let $\mu = \cos\theta$ be the cosine zenith angle of incident radiation with $\mu = +1$ vertically

downward. Following Modest (2013) Section 2.5 Eq. 2.89–2.98, the Fresnel reflectivity and transmissivity to incident (downward) radiation are:

$$R_{\mathrm{F}}(\mu) = \frac{1}{2}\left[\left(\frac{\mu - \mathrm{n}\mu_{\mathrm{n}}}{\mu + \mathrm{n}\mu_{\mathrm{n}}}\right)^2 + \left(\frac{\mathrm{n}\mu - \mu_{\mathrm{n}}}{\mathrm{n}\mu + \mu_{\mathrm{n}}}\right)^2\right] \tag{25}$$

$$T_{\mathrm{F}}(\mu) = 1 - R_{\mathrm{F}}(\mu) \tag{26}$$

where $\mathrm{n} + \mathrm{ik}$ and $\mathrm{n}_0 + \mathrm{ik}_0$ are the complex refractive indices of PVC and air, respectively, and:

$$\mu_{\mathrm{n}} = \sqrt{1 - (1 - \mu^2)/\mathrm{n}^2} \tag{27}$$

is the refracted cosine zenith angle in the PVC pipe. Radiation transmitted into the PVC is attenuated exponentially:

$$\mathrm{a}(\mu_{\mathrm{n}}) = \mathrm{e}^{-\tau/\mu_{\mathrm{n}}} \tag{28}$$

where:

$$\tau = 4\pi kL/\lambda \tag{29}$$

is the optical thickness of the PVC pipe with wall thickness $L = 0.004$ m. Radiation that transmits through L is internally reflected upward from the inner wall in the direction μ_{n} and attenuated exponentially along path length τ. Radiation that reaches the outer wall at $\mu_{\mathrm{n}} < \mu_{\mathrm{c}}$ is transmitted across the outer wall according to $T_{\mathrm{F}}(\mu_{\mathrm{n}})$ and reflected back into the PVC according to $R_{\mathrm{F}}(\mu_{\mathrm{n}})$, where μ_{c} is the critical angle given by Snell's law:

$$\mu_{\mathrm{c}} = \sqrt{1 - 1/\mathrm{n}^2}. \tag{30}$$

Formulas for $T_{\mathrm{F}}(\mu_{\mathrm{n}})$ and $R_{\mathrm{F}}(\mu_{\mathrm{n}})$ are similar to Eq. 25 and Eq. 26 with modifications for total internal reflection about μ_{c} and are given elsewhere (Briegleb and Light, 2007; Liou, 2002).

The total reflectivity is estimated with the successive-order-of-scattering method (van de Hulst, 1980), which accounts for the multiple internal reflections and absorption within the PVC described by Eq. 25–30. We model the PVC pipe as a plane, which is justified because the radius of curvature is much larger than all wavelengths of light considered here. For the geometry and optical properties of the detector rod, the total reflectivity has the closed-form solution:

$$R_{\mathrm{d}} = R_{F,\mu} + \frac{T_{F,\mu} R_{F,\mu_{\mathrm{n}}} T_{F,\mu_{\mathrm{n}}} \mathrm{a}_{\mu_{\mathrm{n}}}^2}{1 - R_{F,\mu_{\mathrm{n}}} a_{\mu_{\mathrm{n}}}^2} \tag{31}$$

where the subscripts μ and μ_{n} on R, T, and a indicate the direction of incident radiance.

S2 Model validation

The Monte Carlo model described above is verified by comparison with benchmark values for total diffuse reflectance R_{d} [W m^{-2}], total transmittance T_{t} [W m^{-2}], diffuse angular reflectance $R_{\mathrm{d}}(\alpha)$ [W sr^{-1}] and diffuse angular transmittance $T_{\mathrm{d}}(\alpha)$ [W sr^{-1}] tabulated by van de Hulst (1980). The angular quantities, which have units of radiant intensity, are defined with respect to the exiting angle normal to the surface α [rad]. For a plane-parallel slab with optical properties $\sigma_{\mathrm{s}} = 0.9$ m^{-1}, $\sigma_{\mathrm{a}} = 0.1$ m^{-1}, $\mathrm{g} = 0.75$, and optical thickness $\tau = 2$, the van de Hulst (1980) solutions are $R_{\mathrm{d}} = 0.09739$ and $T_{\mathrm{t}} = 0.66096$. For an ensemble of $N = 100$ simulations, the Monte Carlo model described

above gives $R_d = 0.09740 \pm 0.00034$ and $T_t = 0.66098 \pm 0.00049$ ($\mu \pm 1\sigma$). The model closely reproduces the benchmark solutions for $R_d(\alpha)$ and $T_d(\alpha)$ (Fig. 7).

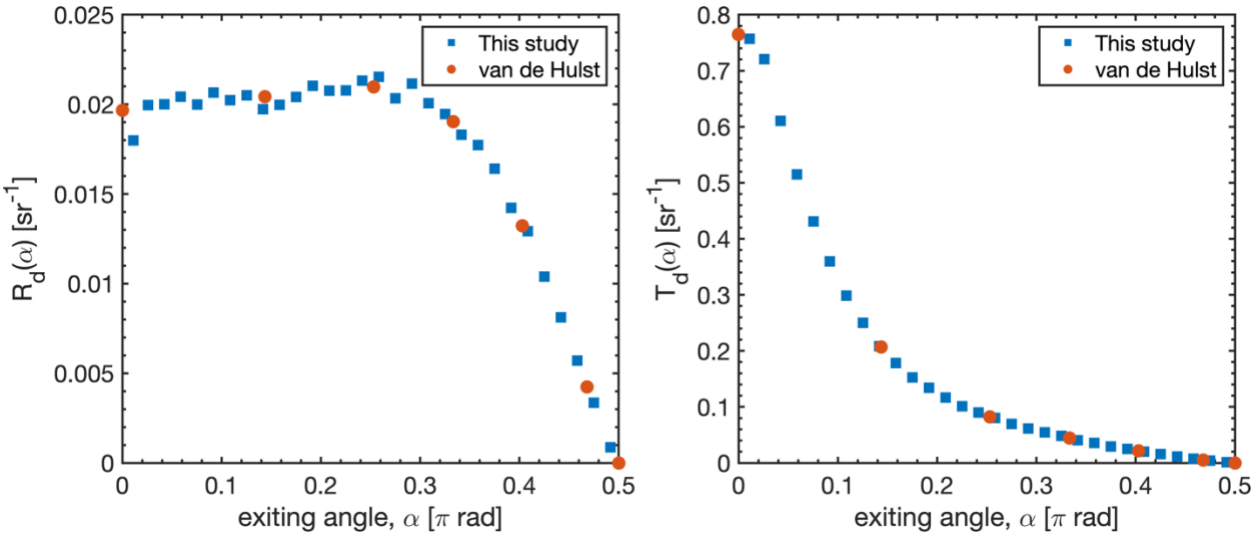

Fig. 7: Values of diffuse angular reflectance (radiant intensity), $R_d(\alpha)$ and transmittance $T_d(\alpha)$ vs. the photon exiting angle with respect to the surface normal α (after Wang et al. 1995 Fig. 3). Solid circles are benchmark solutions from Table 35 in van de Hulst (1980), obtained with the doubling method of solution to the radiative transfer equation.

S3 Monte Carlo uncertainty estimate

The Monte Carlo model is used to estimate the effect of detector interference on our irradiance measurements and, in turn, the asymptotic flux attenuation coefficients k_{att} that are estimated from them. To this end, we designed four experiments that isolate two forms of detector interference: 1) the non-ideal cosine response of the irradiance detector, and 2) absorption and scattering by the PVC detector rod. The four experiments, including a base simulation with no detector interference, are summarized in Table S1.

Table S1: Summary of four Monte Carlo experiments that simulate the effect of the detector rod interference on in-ice irradiance measurements. The baseline simulation (ideal diffusion, no rod) has no detector interference.

Experiment	Source function	Detector absorption	Detector scattering
Ideal Diffusion, No Rod	Eq. 23-24	-	-
Ideal Cosine, No Rod	Eq. 22	-	-
Ideal Cosine, With Rod	Eq. 22	ω_{rod}	Eq. 23-24
Non-ideal Cosine, With Rod	Empirical (Fig. 6)	ω_{rod}	Eq. 23-24

For each experimental setup, the Monte Carlo is integrated across 10,000 interactions at four wavelengths (400 nm, 500 nm, 600 nm, and 700 nm) with detector rod positions that are identical to the measurement depths reported in this paper (c.f. Fig. 5). For the 20 July experiment, these depths are 9.35 cm, 30.0 cm, 50.45 cm, and 68.60 cm, in units of solid-ice equivalent (i.e., physical thickness scaled by measured ice density). For the 21 July experiment, these depths

are 45.93 cm, 58.98 cm, 73.40 cm, and 114.5 cm. Monte Carlo k_{att} values are estimated for each wavelength with the same method used for the field-estimates, i.e., by least-squares linear regression:

$$-\log T(\mathrm{z},\lambda) = T_0 + k_{\mathrm{att}}(\lambda)\mathrm{z} + \varepsilon \tag{32}$$

where T is the total diffuse transmittance from Monte Carlo simulation (see Section S2), T_0 is a parameter (y-intercept) that represents $T(\mathrm{z}=0)$ and ε is an error term.

These simulations provide two measures of k_{att} uncertainty: 1) the difference between the average Monte Carlo k_{att} value μ_{MC} and the field-estimated k_{att} value at each wavelength, and 2) the spread among Monte Carlo k_{att} values at each wavelength. The spread among Monte Carlo k_{att} values is an estimate of uncertainty due to the irradiance sensor angular response function and the detector rod interference. The spectrometer dark-light sensitivity is an additional source of instrumental uncertainty that is estimated from field measurements as described in Sect. X. These instrumental uncertainties (irradiance sensor angular response, detector rod interference, and dark-light sensitivity) are compared with the statistical variations in the high-frequency irradiance measurements and with the statistical uncertainty in the k_{att} linear regression model (Eq. 32).

If we take the spread among the Monte Carlo k_{att} values as independent of the uncertainty estimates obtained from analysis of field datasets and the uncertainty in the linear regression model, a combined uncertainty is estimated as:

$$\varepsilon = \sqrt{\varepsilon_{MC}^2 + \varepsilon_D^2 + \varepsilon_{2\sigma}^2 + \varepsilon_{LM}^2} \tag{33}$$

where ε_{MC}, ε_D, $\varepsilon_{2\sigma}$, and ε_{LM} are the uncertainty from Monte Carlo, dark-current sensitivity, high-frequency statistical variability, and linear model statistical uncertainty, defined as one standard error in the k_{att} linear regression (Fig 8).

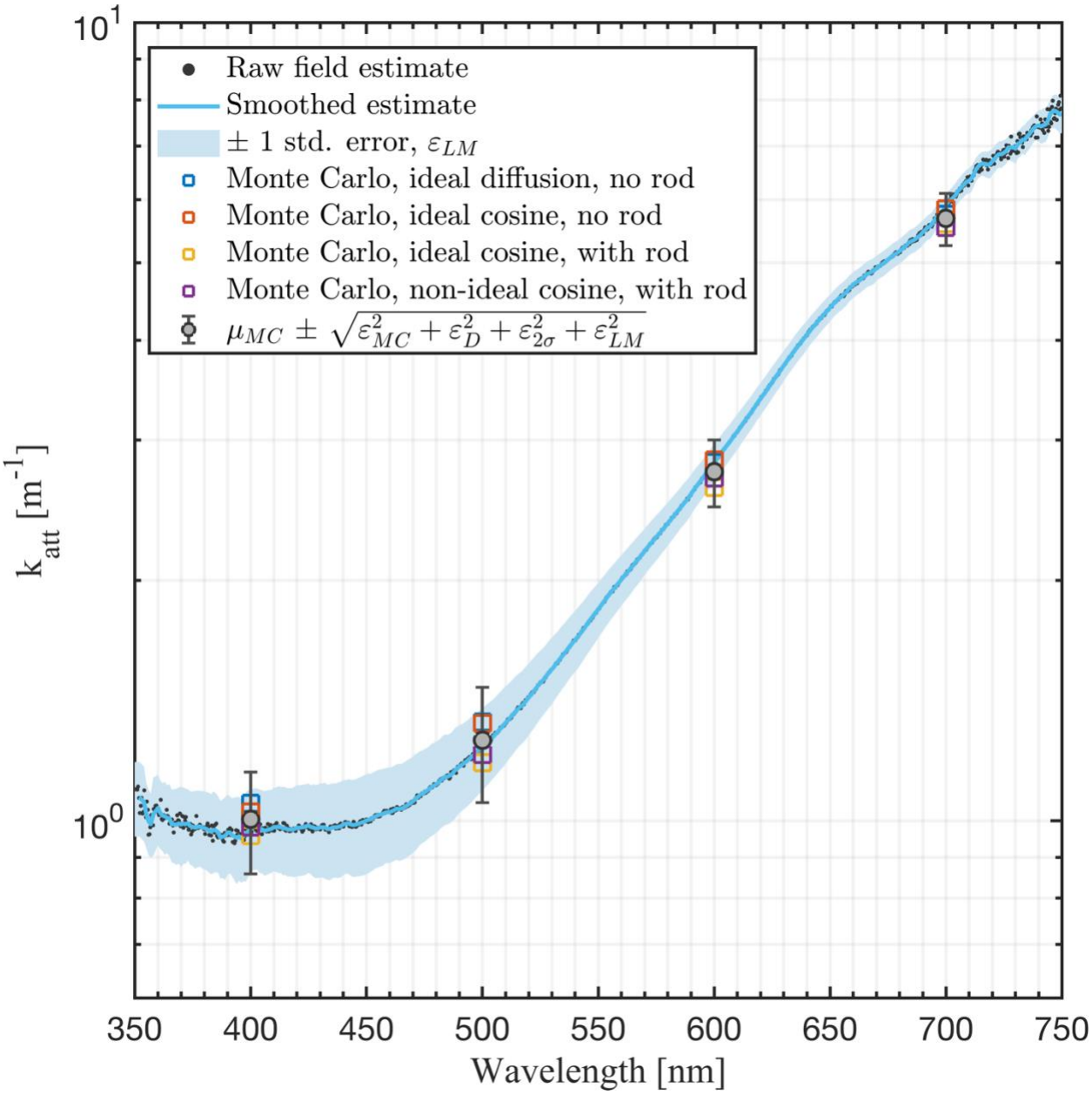

Fig 8: Attenuation coefficient k_{att} spectra from measurements of light transmission collected on 20 July, 2018, compared with average k_{att} values from four simulations with a 3-dimensional Monte Carlo radiative transfer model (μ_{MC}) and with two measures of uncertainty: 1) statistical linear model uncertainty ε_{LM} (shaded uncertainty bounds; ±1 standard error in the linear regression) and, 2) ε_{LM} combined with instrumental and measurement uncertainty (error bars; $\mu_{MC} \pm \varepsilon$). The combined estimate combines ε_{LM} with uncertainty due to spectrometer dark-light sensitivity, non-ideal cosine response of the irradiance sensor, detector rod interference, and statistical variations in the high-frequency raw data (±2 standard deviations).

References

Briegleb, B. P. and Light, B.: A Delta-Eddington Mutiple Scattering Parameterization for Solar Radiation in the Sea Ice Component of the Community Climate System Model, Technical Note, National Center for Atmospheric Research, Boulder, Colorado. [online] Available from: http://dx.doi.org/10.5065/D6B27S71 (Accessed 18 February 2019), 2007.

Ertürk, H. and Howell, J. R.: Monte Carlo Methods for Radiative Transfer, in Handbook of Thermal Science and Engineering, edited by F. A. Kulacki, pp. 1–43, Springer International Publishing, Cham., 2017.

Gordon, H. R.: Ship perturbation of irradiance measurements at sea 1: Monte Carlo simulations, Appl. Opt., 24(23), 4172, doi:10.1364/AO.24.004172, 1985.

van de Hulst, H. C.: Multiple light scattering: tables, formulas, and applications, Academic Press, New York., 1980.

Leathers, R. A., Downes, T. V., Davis, C. O. and Mobley, C. D.: Monte Carlo Radiative Transfer Simulations for Ocean Optics: A Practical Guide, Memorandum, Naval Research Laboratory, Washington, D.C. [online] Available from: https://www.oceanopticsbook.info/packages/iws_l2h/conversion/files/Leathersetal_NRL2004.pdf (Accessed 11 October 2020), 2004.

Light, B., Maykut, G. A. and Grenfell, T. C.: A two-dimensional Monte Carlo model of radiative transfer in sea ice, J. Geophys. Res. Oceans, 108(C7), 3219, doi:10.1029/2002JC001513, 2003.

Liou, K.-N.: An introduction to atmospheric radiation, 2nd ed., Academic Press, Amsterdam ; Boston., 2002.

Modest, M. F.: Radiative heat transfer, Third Edition., Academic Press, New York., 2013.

Mullen, P. C. and Warren, S. G.: Theory of the optical properties of lake ice, J. Geophys. Res. Atmospheres, 93(D7), 8403–8414, doi:10.1029/JD093iD07p08403, 1988.

Wang, L., Jacques, S. L. and Zheng, L.: MCML—Monte Carlo modeling of light transport in multi-layered tissues, Comput. Methods Programs Biomed., 47(2), 131–146, doi:10.1016/0169-2607(95)01640-F, 1995.

Zhang, X., Qiu, J., Li, X., Zhao, J. and Liu, L.: Complex refractive indices measurements of polymers in visible and near-infrared bands, Appl. Opt., 59(8), 2337, doi:10.1364/AO.383831, 2020.